In Situ Photophysical Characterization of π-Conjugated Oligopeptides Assembled via Continuous Flow Processing

Lawrence R. Valverde,[†] Bo Li,[‡] Charles M. Schroeder,[†,‡] and William L. Wilson*[,†,§,∥]

[†]Department of Materials Science and Engineering, University of Illinois at Urbana-Champaign, 1304 West Green Street, Urbana, Illinois 61801, United States
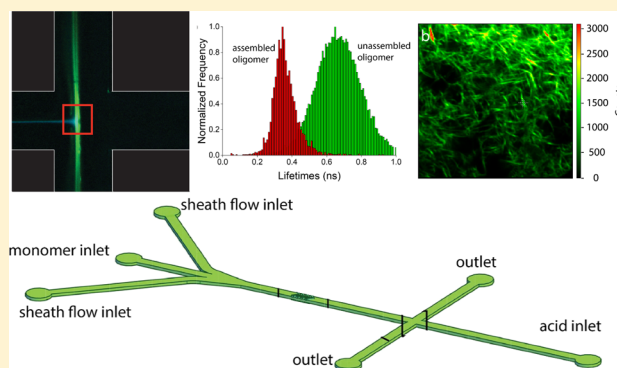
[‡]Department of Chemical and Biomolecular Engineering, University of Illinois at Urbana-Champaign, 600 South Mathews Avenue, Urbana, Illinois 61801, United States

[§]Frederick Seitz Materials Research Laboratory, University of Illinois at Urbana-Champaign, Urbana, Illinois 61801, United States

[∥]Center for Nanoscale Systems, Faculty of Arts and Sciences, Harvard University, Cambridge, Massachusetts 02138, United States

ⓢ *Supporting Information*

ABSTRACT: Bioinspired materials have been developed with the aim of harnessing natural self-assembly for precisely engineered functionality. Microfluidics is poised to play a key role in the directed assembly of advanced materials with ordered nano and mesoscale features. More importantly, there is a strong need for understanding the kinetics of continuous assembly processes. In this work, we describe a continuous microfluidic system for the assembly and alignment of synthetic oligopeptides with π-conjugated cores using a three-dimensional (3D) flow focusing of inlet reactant streams. This system facilitates in situ confocal fluorescence microscopy and in situ fluorescence lifetime imaging microscopy (FLIM), which can be used in unprecedented capacity to characterize the integrity of peptides during the assembly process. To achieve continuous assembly, we integrate chevron patterns in the ceiling and floor of the microdevice to generate a 3D-focused sheath flow of the reactant peptide. Consequently, the peptide stream is directed toward an acidic triggering stream in a cross-slot geometry which mediates assembly into higher-order fiber-like structures. Using this approach, the focused peptide stream is assembled using a planar extensional flow, which ensures high degrees of microstructural alignment within the assembled material. We demonstrate the efficacy of this approach using three different synthetic oligopeptides, and in all cases, we observe the efficient and continuous assembly of oligopeptides. In addition, finite element simulations are used to guide device design and to validate 3D focusing. Overall, this approach presents an efficient and effective method for the continuous assembly and alignment of ordered materials using microfluidics.

INTRODUCTION

Naturally occurring polymers such as DNA, RNA, and peptides can deterministically self-assemble into complex hierarchical three-dimensional (3D) structures that give rise to specific functions. In recent years, bioinspired materials have been developed with the aim of harnessing natural self-assembly for precisely engineered functionality.[1−3] The development of new biomimetic materials has benefitted from advances in both synthetic organic chemistry and the improved synthesis of biological materials.[1−11] Nonetheless, the development of systematic methods for controlling the nano to mesoscale ordering of functional materials remains a challenge. To control structural ordering, biohybrid materials such as functionalized oligopeptides are typically processed in batch solutions and deposited onto surfaces to generate functional devices using a variety of methods including spin-coating,[2,12,13] electrospinning,[2,14−18] and roll-to-roll template

printing.[13] However, it is challenging to use these methods to optimally align ordered domains such as π-conjugated units at the molecular scale. To this end, there is a need for the continued development of new methods for the directed self-assembly of engineered materials, especially for organic semiconductor applications.

Microfluidic devices have played an increasingly important role in the fabrication of supramolecular assemblies.[19−27] Simple cross-slot microdevices can provide access to nanoscale control over substructure alignment. However, current methods suffer from unwanted material buildup and channel obstruction, precluding in situ characterization, and limiting throughput while causing uncertainty in the prior processing

history of the collected assembled material.[2] These problems are rooted in the undesirable nonspecific adsorption of the assembled material on the device's inner surfaces, precluding the continuous, high-throughput assembly of peptides in flow. In such context, microfluidic methods for 3D flow focusing have been developed for applications such as improved flow cytometry.[14,16,28−35] While the most straightforward approach involves top and bottom focusing streams in an analogous fashion to more common 2D lateral focusing streams, groove- or chevron-patterned microchannels can provide controllable sheathed flows without the need for more complicated 3D lithographic techniques or additional fluidic sources or pumps.[14,16,28,30,32,33]

In this work, we implement 3D flow focusing of peptide streams using patterned microfluidic channels for the novel application of achieving continuous assembly of oligopeptides. This innovation enables the unprecedented characterization of the material and its assembly in situ as well as direct confirmation of previous hypotheses regarding the assembled product alignment. In particular, we incorporate chevron structures into the ceiling and floor of the inlet channels in cross-slot microdevices such that the reactant peptide stream is focused before reaching the assembly zone at the cross-slot region, enabling the device-mediated assembly for high throughput deposition techniques such as ink jet and e-jet printing. For these devices, microfluidic channel designs are validated using computational fluid dynamics and chemical transport simulations in COMSOL. As a result, flow focusing and real-time assembly were characterized in situ using confocal fluorescence microscopy, polarized fluorescence microscopy, and in situ and ex situ fluorescence lifetime imaging microscopy (FLIM). In all cases, we observe the unobstructed continuous assembly and alignment of synthetic oligopeptides over long times. We furthermore spatially correlate lifetime signals from unassembled and aligned, assembled material as it forms in situ. Finally, we indicate two paradigms in which printing can be developed and integrated with our current device for future high-throughput materials processing and deposition. Taken together, our results show that the integrated chevron/cross-slot microdevices offer the potential for new microreactor designs with enhanced control over fluid flow to generate the assembled materials in a continuous flow format.

■ EXPERIMENTAL SECTION

Microdevice Fabrication. Microfluidic cross-slot devices with chevron patterns were fabricated using standard soft lithography techniques.[36,37] Microdevices consist of hybrid glass/poly-(dimethylsiloxane) (PDMS) assemblies suitable for fluorescence microscopy. Chevrons were designed with a 90° angle and were symmetrically centered along the top and bottom of the inlet oligopeptide stream. Chevron dimensions were 50 μm in height by 50 μm in width with a 200 μm pitch, and channel dimensions were 100 μm in height by 400 μm in width (Figure 2). Overall, the integrated PDMS device consists of three layers (top chevrons, center channels, and bottom chevrons), which requires careful alignment of these features. Two different masters were created on silicon wafers using SU-8 photoresist (MicroChem) and exposed to UV light with a custom photomask (MRL photomask services). One master was created by first spin-coating a 100 μm-thick layer of SU-8 and exposing and developing the pattern for the main (center) channel features. Next, a 150 μm-thick layer of SU-8 was deposited, and the chevron photomask was aligned with the monomer inlet channels using a stereomicroscope. The pattern was then exposed and developed to reveal a two-layer master containing the aligned channel

and top-chevron features. A second master was created using standard techniques and contained a single layer of 100 μm-tall chevrons, which would serve to create the bottom layer chevrons in the inlet channel. Both masters were then treated with chlorotrimethylsilane (Sigma-Aldrich) vapor to prevent PDMS adhesion. Approximately 30 g of PDMS mixed in a ratio of 10:1 base/cross-linker was poured into a standard Petri dish containing the two-layer master. Separately, a 50 μm-thick layer of the same PDMS solution was spin-coated onto the second master, thereby resulting in the master's SU-8 chevron features protruding 50 μm above the PDMS layer. The excess 50 μm height of the one-layer chevron master served to ensure that the spin-coated PDMS did not seal off the chevron features and to aid in the lateral alignment of layers by protruding slightly into the channel of the two-layer mold. After baking both molds for ∼20 min at 60 °C the two-layer portion was removed from the master, inlet and outlet holes were punched through the layers, and a stereomicroscope was used to align the channels and top chevrons of the two-layer PDMS mold with the chevron features of the 50 μm spin-coated mold. After an overnight cure, PDMS was removed from the master and bonded to glass coverslips by treatment in oxygen plasma.

Fluidic-Directed Assembly of Synthetic Oligopeptides. Flow-focused streams of unassembled oligopeptide at a concentration of 0.1 mM in deionized water (18.2 MΩ·cm) were introduced into cross-slot devices and directed against an opposing aqueous acidic stream of 10 mM HCl, such that these two streams meet at the cross-slot junction (Figure 2). The unassembled peptide stream (volumetric flow rate 10 μL/min) was first focused laterally in 2D using two flanking streams of deionized water (500 μL/min). The 2D focused peptide stream was then directed into the inlet channel containing chevron features in the ceiling and floor, thereby resulting in a 3D flow-focused peptide stream. An aqueous acidic stream was introduced into the opposing inlet at the cross-slot junction at a volumetric flow rate of 500 μL/min and later slowed to 250 μL/min in order to shift the position of the oligomer assembly front. In order to facilitate assembly, we initiated flow conditions in the following order: focusing stream, unassembled peptide stream, aqueous acid stream, followed by terminating the process using the reverse procedure. This order of operations significantly reduces the introduction of air bubbles in the cross-slot or chevrons and/or backflow of the acid stream into the monomer solution that could result in unwanted spontaneous assembly. Three Harvard apparatus PHD ULTRA syringe pumps were used to generate fluid flow. Forked tubing was used to connect the two cross-slot outlets to a single outlet from which the effluent stream was collected.

Fluorescence and Confocal Microscopy. Microdevices were mounted on a Zeiss LSM 700 inverted microscope and imaged through a 5× EC Plan-Neofluar objective (NA = 0.16) onto a linear CCD array (512 × 512 pixels). The peptides investigated in this work exhibit a blue-shifted absorption and quenched red-shifted emission upon assembly. For this reason, the images were acquired by splitting fluorescence emission into two channels using appropriate dichroic mirrors, band-pass filters, and long-pass filters to distinguish the assembled oligomer from the unassembled peptide (Table S1). Confocal images were acquired through a slit approximately 1 Airy unit wide (∼10 μm) with a galvo y-scan and raster laser line oriented in the x-direction and scanned in the z-direction using a fast-scanning piezo-collar objective.

Ex Situ Fluorescence Lifetime Imaging Microscopy (FLIM). The samples were prepared by pipetting a small amount (∼15 μL) of material collected from the outlet stream of a microfluidic device onto glass slides, followed by addition of a glass coverslip and sealing with clear nail polish. Glass microscope slides were then mounted on a Nikon Eclipse Ti inverted microscope in conjunction with an Alba FCS and scanning mirror module. A mode-locked Ti:sapphire laser system (Tsunami and Millennia, Spectra-Physics) was used for two-photon illumination of the samples at 80 MHz pulse repetition rate with ∼100 fs pulse width. Fluorescence emission was imaged using a Nikon Plan APO 60× objective lens (NA = 1.2) and a single-photon counting module with sensitivity from ∼500 to 1100 nm (70% quantum efficiency peak at 650 nm, dark count = 50 counts s^{-1}). Data
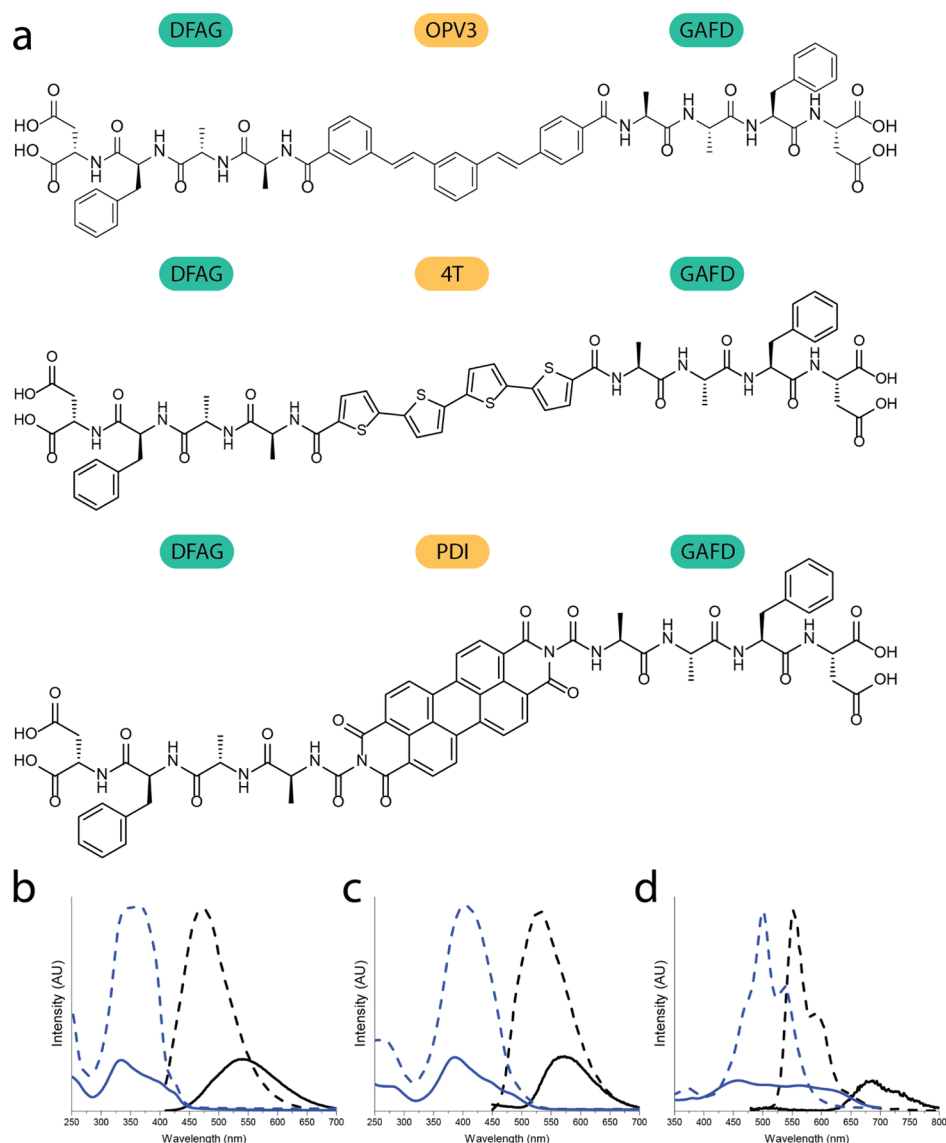
Figure 1. Photophysical properties of synthetic oligopeptides. (a) Structures and (b–d) bulk spectral properties of synthetic oligopeptides with different π-conjugated cores flanked by symmetric DFAG residues. Absorption and fluorescence emission spectra are shown for: (b) DFAG-OPV3, (c) DFAG-4T, and (d) DFAG-PDI. Absorption spectra (blue dashed lines) and fluorescence emission spectra (black-dashed lines) are shown for oligopeptides under basic solution conditions prior to assembly. Under acidic conditions (pH < 3), these synthetic oligopeptides assemble into fiber-like networks that exhibit blue-shifted absorption peaks (solid blue lines) and red-shifted emission (solid black lines).

were analyzed for fluorescence lifetimes using ISS VistaVision software.

In Situ Fluoresence Lifetime Imaging Microscopy (FLIM). Microdevices were mounted on a Zeiss LSM710 inverted microscope and imaged through a Zeiss Plan-Apochromat 20× objective (NA = 0.8). A Ti:sapphire laser system (Mai Tai, Spectra-Physics) was used for two-photon illumination of the devices. The FLIM system was first calibrated using ISS Vista software and a rhodamine 6G standard (lifetime = 4.03 ns). The edge of a drop of rhodamine dye was focused onto one of two highly sensitivity non-descanned (GaAsP) detectors and then directed to single-photon counting modules (ISS) for system calibration. Following the microdevice setup and flow initiation, the cross-slot device was imaged using a QUASAR 34 channel spectral detector, consisting of two standard photomultiplier tube (PMTs) and a 32 channel PMT array. Once the assembly was verified, the scan area and speed were decreased to a 256 × 256 array with a 6.3 μs-pixel dwell time at a 2× zoom, and the light path was redirected toward the single-photon counting modules. Data were analyzed for fluorescence lifetimes using the ISS VistaVision software, similar to ex situ data.

Computational Modeling. We performed a series of simulations of the flow process using computational fluid dynamics to assess the effect of chevron features on flow focusing in microfluidic channels. Moreover, the simulations further served to inform the requisite number and spacing of chevrons for efficient 3D flow focusing. In particular, we used finite element analysis in COMSOL Multiphysics to analyze flow fields generated by grooved channel features. The computational algorithm considers the Navier–Stokes equations for incompressible flow in the laminar flow regime, for which nonlinear inertial terms can be neglected

$$-\frac{\partial p}{\partial x_i} + \mu \frac{\partial^2 u_i}{\partial x_j \partial x_j} = 0$$

$$\frac{\partial u_i}{\partial x_i} = 0 \tag{1}$$

where p is the pressure, u_i is the fluid velocity, and μ is the dynamic viscosity. Equation 1 is given in indicial notation such that subscripts refer to vector components. For the dilute aqueous streams, we used
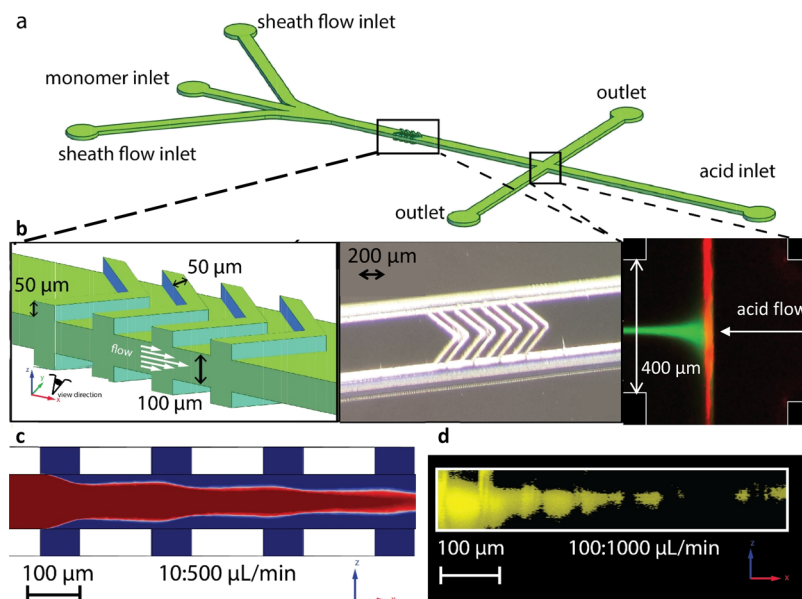
Figure 2. Integrated microfluidic device with a cross-slot channel geometry and chevron features for 3D-focused oligopeptide assembly and alignment. (a) Schematic of the chevron microdevice. (b) Left: Close-up schematic of the chevron patterns. Center: Optical micrograph of the aligned chevrons. Right: False color image showing the cross-slot microdevice in operation for the DFAG-PDI assembly as viewed under 50× objective. (c) COMSOL simulation results showing vertical flow focusing of a core stream (red) using a sheath flow (blue). (d) Side view of a reconstructed confocal microscope 3D image of flow focusing for a fluorescent dye at a core/sheath flow ratio of 1:10.

standard properties for water at ambient temperature with no-slip boundary conditions at the walls, laminar inflow boundary conditions at the inlets, and open interface boundary conditions at the outlets. The transport of the dilute species module of COMSOL was used to model diffusion via Fick's law

$$\frac{\partial}{\partial x_j}\left[D\frac{\partial c}{\partial x_j} - cu_j\right] = 0 \tag{2}$$

where D is the diffusion coefficient and c is the concentration of the focused species (small molecule dye or unassembled peptide oligomer). We assume a constant diffusion coefficient D and use a normalized concentration c such that $c = \tilde{c}/\tilde{c}_0$, where $\tilde{c}$ is the dimensional concentration and $\tilde{c}_0$ is the dimensional inlet concentration. It is assumed that the peptide monomer is sufficiently dilute such that the presence of the dissolved peptide in the flowing streams does not influence fluid flow. In this way, we first solved the Navier–Stokes equations and then used the flow solution as the velocity field for solving the associated convection-diffusion problem.

Ligler and co-workers[32] previously investigated the impact of grooved chevron features in generating sheath flows in microfluidic channels. In particular, prior work provides a comprehensive analysis of the effects of both the number and spacing of chevrons on 3D flow focusing. In general, the number of chevrons controls the vertical compression (z-direction focusing), whereas the sheath-to-core flow ratio controls the lateral focusing, with various permutations affecting the shape of the focused stream. Higher flow ratios of sheath-to-core change the shape of the core stream from bowtie-like to oblong to nearly circular focusing. In the present work, we were primarily interested in generating a simple sheath flow in order to exclude the focused peptide stream from the top and bottom surfaces, hence the details of the shape of the focused stream were not critical for our purposes. For these reasons, we generally employed sets of four chevrons in our devices using a specific pattern that was found to be efficient for flow focusing in prior works (chevrons with a 90° angle, symmetrically centered along the top and bottom of the inlet stream, with similar dimensions to those used in this study).

RESULTS

Photophysics of Synthetic Peptides with Different Functional Cores. In this work, we studied the fluidic-directed assembly of three different synthetic peptides containing the same flanking amino acid sequence but with three different cores: OPV3, quaterthiophene (4T), and perylene-diimide (PDI) (Figure 1). These oligopeptides consist of a π-conjugated core flanked on either side with symmetric peptide sequences DFAG (aspartic acid, phenylalanine, alanine, glycine). The dashed lines in Figure 1 spectra are for oligopeptides under basic solution conditions prior to assembly. Under acidic conditions, these peptides assemble into supramolecular fibers (Figure S1) via β sheet formation due to pH-triggered electrostatic screening of aspartic acid residues that become protonated below the pK_a of the residue side chain, thereby facilitating hydrogen bonding and van der Waals interactions between oligopeptides. β sheet formation can be further influenced by the solvation and π−π interactions of the cores, depending on the chemical identity of the π-conjugated core.[1,2,5,9]

We began by characterizing the photophysical properties of these three synthetic oligopeptides with different π-conjugated cores: OPV3, 4T, and PDI (Figure 1a). Upon assembly, these peptides exhibit blue-shifted absorption peaks (solid blue lines in Figure 1) and quenched red-shifted fluorescence emission (solid red lines in Figure 1), which is consistent with H-aggregate formation in the framework originally developed by Kasha and co-workers and expanded upon by Spano and co-workers.[2,38] The red-shifted fluorescence emission for 4T-functionalized peptides is noticeably less pronounced compared to peptides with OPV3 and PDI cores, which necessitates the use of different optical configurations for fluorescence imaging of peptides with 4T cores (Figure 1b,c, Table S1). Furthermore, the PDI peptide exhibits a significantly quenched fluorescence emission relative to 4T or OPV3 peptides due to its more n-type properties, which
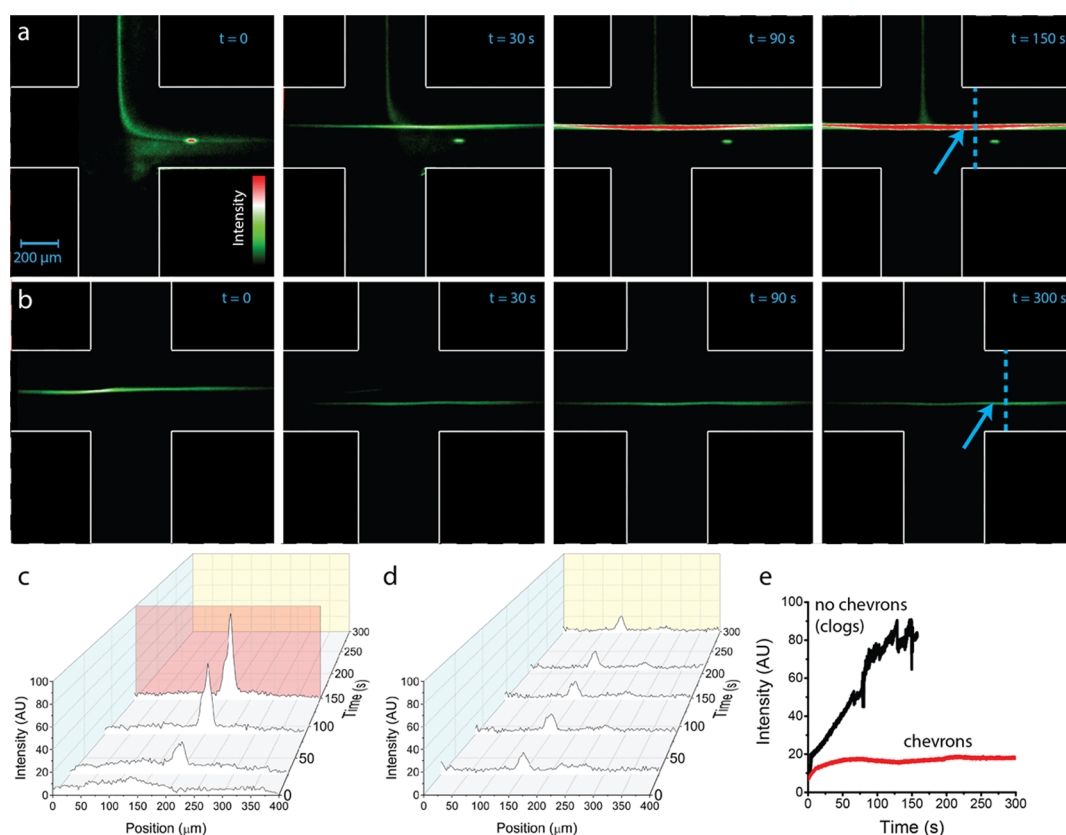
Figure 3. Assembly of oligopeptides in cross-slot microdevices. (a) Time series of fluorescence images showing an assembly of DFAG-OPV3 peptides in a simple cross-slot microdevice without chevrons. (b) Time series of fluorescence images showing an assembly of DFAG-OPV3 peptides in a simple cross-slot microdevice with chevrons. Images are shown in a false color intensity map normalized to the highest intensity across all images. (c) Fluorescence intensity line scan from the microdevice without chevrons across an outlet channel immediately downstream of the cross-slot indicated by a blue dashed line in the image in panel (a). (d) Fluorescence intensity line scan from a microdevice with chevrons across an outlet channel immediately downstream of the cross-slot indicated by a blue-dashed line in the image in panel (b). (e) Fluorescence intensity of a 15 μm diameter spot centered on the assembly front, indicated by the blue arrow in the fluorescence images in (a,b) as a function of time.

complicates the detection of PDI-assembled peptides (Figure 1d). For these reasons, we primarily focused on OPV3-functionalized peptides for characterizing assembly dynamics via fluorescence spectroscopy, though all three are assembled using the new continuous flow microdevices.

Flow Field Characterization for 3D Flow Focusing. Diagonal groove patterns (chevrons) were used in the ceilings and floors of microdevice inlet channels to generate a sheath flow consisting of an inner peptide stream enfolded in an outer sheath stream (Figure 2). The sheath stream is introduced at a higher volumetric flow rate than the inner core stream so that sheath fluid is directed across the channel above and below the inner peptide stream, thereby inducing vertical displacement and compression of the inner fluid. In particular, we used symmetric pairs of chevron patterns, four on top and four on bottom of the peptide inlet stream (Figure 2a,b), in order to maintain the sample stream symmetry at the cross-slot and to generate coaxial flows that are fairly insensitive to the sheath-to-core flow rate ratio.[14,32] The channels are 400 μm wide by 100 μm tall with chevrons that are 50 μm tall and 50 μm wide with a 90° apex, intersecting the channel walls at a 45° angle. Following flow focusing, the peptide stream is directed to a 4-channel microfluidic cross-slot. In the vicinity of the cross-slot, the field is planar extensional with a fluid velocity described by $v_y = \dot{\varepsilon}y$ and $v_x = -\dot{\varepsilon}x$, where $\dot{\varepsilon}$ is the strain rate and (x, y) are the distances along the inlet (or outlet) from the stagnation point at the center of the cross-slot. In this way, peptide

assembles due to diffusive mixing at the interface between the unassembled peptide and acid streams in the cross-slot junction. In addition, by making the diffusive interface coincide with the extensional flow axis, the extensional component of the flow pulls and aligns the products as they assemble.[2,39] Using this integrated microfluidic device, we effectively generated 3D flow-focused inlet streams for OPV, 4T, and PDI peptides, followed by peptide assembly and alignment in a continuous flow format over long times (Figures 2b and S7a–c). The inlet peptide stream (green, unassembled) is directed from left to right. The assembled peptide flows in the vertical outflow channels and appears with a red-shifted fluorescence emission. Red color is used to illustrate the emission wavelengths redder than the dichroic cutoff and green is used for emission that is bluer. Fluorescence emission was detected using the optical configurations described in Table S1.

Before proceeding with assembly experiments, we assessed the performance of microdevice designs using computational fluid dynamics in COMSOL Multiphysics. In particular, we evaluated the performance of these devices for 3-D focusing using sheath-to-core flow ratios in the range of 10:1−100:1 (Figure 2b,c). Flow focusing is achievable by maintaining a flow with a Reynolds number around 100 or below, and while this is accomplished primarily through the small dimensions of the device, it is also necessary to maintain overall flow rates on the order of 1 mL/min at most.[40] By maintaining a sample

flow rate of ~10 μL/min, we could vary the focusing streams between 100 and 1000 μL/min and maintain the necessary flow regime. The ratio between these flow rates is also responsible for the shape and size of the resulting focused stream. Relatively lower sheath flow rates yield a horizontal dog bone shape that can be inadequately separated from the devices' ceiling and floor at the dog bone lobes, while the most aggressive sheath flow rates can create an hourglass shape suspended at the flow center but this nearly bifurcates the focused stream along the horizontal axis. Sheath flow rates between ~250 and 500 μL/min provide symmetric square-like coaxial focusing. There is also some latitude in deciding the number of chevrons to use as there is increased focusing, but also increased flattening, of the focused stream as it passes through each successive chevron. One could also envision varying the depths, widths, and angles of the chevrons, but we did not investigate these other parameters. We found that the four-chevron microdevice geometries and operating parameters detailed herein were suitable for our goal of achieving efficient sheathing of the inner peptide stream, which effectively prevents the peptide from interacting with the top and bottom surfaces of microdevices while maintaining lateral focusing (Figure 2c).

Following the validation of microdevice designs, we next fabricated three-layer-integrated microfluidic devices containing the same chevron patterns as analyzed in the computational studies. Using these devices, we experimentally characterized the performance of the chevron-containing microdevices for vertical flow focusing of small molecule dye and peptide streams using confocal microscopy. We first introduced a small molecule fluorescent dye as the inner core stream and used water as the sheath stream to demonstrate a proof-of-principle validation of 3D flow focusing. In all cases, we observed efficient vertical focusing and generation of a sheath flow (Figure 2d). Notably, we observed that the higher volumetric flow ratios of sheath-to-core streams resulting in the substantial compression of the inlet dye stream also reduced photon counts to a lower level by decreasing optical path length through the fluorescent material, thereby signifying efficient z-direction focusing before confirmation through confocal z-stack imaging. Using this method, we observed long-term stability (minutes to tens of minutes) of vertically focused streams when operating in a continuous flow mode, which enables the data acquisition using confocal imaging for the vertical z-stack image integration with suitably long exposure times.

Oligopeptide Assembly under Continuous Flow. Following microdevice characterization, we studied the continuous flow assembly of the synthetic oligopeptides (Figures 3 and S2). For these experiments, we introduced a deionized water stream into the sheath flow inlets, an aqueous solution of an unassembled peptide oligomer (0.1 mg/mL) into the sample inlet stream, and an aqueous acidic stream (10 mM HCl) into the opposing inlet channel of the cross-slot junction, as shown in the schematic in Figure 2. For direct comparison, we characterized the assembly of peptides in microdevices without (Figure 3a) and with (Figure 3b) chevron features in the floors and ceilings of the inlet peptide streams. In all cases, microfluidic devices without vertical focusing exhibited rapid peptide aggregation and adhesion to the channel surfaces; assembled oligopeptide begins to form within the first minute and significant adhesion to channel surfaces is visible in less than 2 min (Figure 3a,c). For

microdevices without chevrons, fluorescence intensity measurements in the outlet channels clearly demonstrate the uncontrolled accumulation of the assembled peptide. On the other hand, microdevices containing chevrons allowed for the continuous and long-time assembly of oligopeptides without material accumulation (Figure 3b,d). In Figure 3b at t = 0 s flow rates are adjusted to be equal to the conditions in Figure 3a. At t = 30 s, the assembly front shows oligopeptide formation along new extensional flow axis. Continuous assembly in a steady state as seen in Figure 3b,d can be achieved in microdevices with chevrons over the course of minutes to hours. The experiments in Figure 3a,b were run under identical conditions in terms of peptide and acid concentrations (0.1 mg/mL and 10 mM, respectively) and volumetric flow rates (10 and 500 μL/min for sample and lateral aqueous focusing stream, respectively, and 500 μL/min for the acid stream). The images are shown in a false color intensity map normalized to the highest intensity across all images.

Figure 3e shows the time-dependent fluorescence emission intensity for microdevices with and without vertical flow focusing. In the original devices without chevrons, solutions containing the OPV3-functionalized peptide showed a dramatic accumulation of material with significant clumping after only 90 s of device operation. Prior work has demonstrated that the assembled oligomer in solution will rapidly disassemble when the pH is returned to neutral, nonaggregate-inducing conditions.[2] However, when the acid flow rate was reduced after 2 min from 500 to 250 μL/min, thereby moving the assembly front and enveloping the pre-assembled material in the high pH solution, significant quantities of adhered oligomer aggregation remained, which indicates that the surface-bound or "clumped" assembled material may be irreversibly adhered to the microdevice surfaces (Figure S3). On the other hand, microdevices containing chevrons showed no evidence of aggregation or irreversible adhesion to device surfaces, even after continuous flow and peptide assembly in excess of 15 min. Figure 3d shows that a steady-state amount of the assembled peptide formation is attained within the flow, and the lateral and vertical width of the assembly front does not change in the x–y plane or in the z-direction. This is further evidenced by the constant transient fluorescence emission intensity over long times in the assembled peptide region in microdevices containing chevron features (Figure 3e). Moreover, we found that oligopeptides with 4T and PDI cores exhibited similar behavior to OPV3-functionalized peptides. In microdevices without chevrons, both peptide solutions show evidence of oligomer aggregation and clumping on the top and/or bottom surfaces after only ~150 s of device operation. In contrast, microdevices containing chevrons yield efficient continuous assembly of 4T and PDI peptides for long times (Figure S2).

Characterization of the Acid-Mediated Self-Assembly of Oligopeptides Using FLIM. Continuous fluid-directed assembly in microdevices allows us to directly characterize the properties of assembled materials in real-time using in situ FLIM. Before this development, understanding of peptide assembly, and particularly its alignment, relied upon inference from the collected material. In brief, FLIM measurements provide the time delay between excitation and fluorescence emission. Lifetimes are determined by the available energy state transitions before radiative emission in the sample and are thus indicative of the molecular scale order.
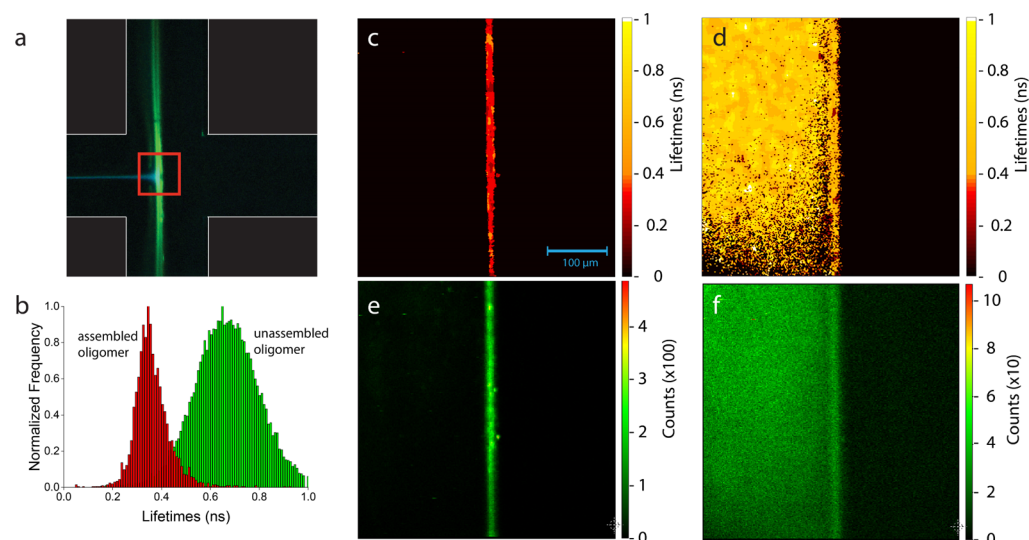
Figure 4. In situ FLIM for fluid-directed assembly of oligopeptides with 4T cores. (a) False color image of the assembly process at device cross-slot (blue shows unassembled peptide and green shows assembled peptide). Red square indicates position and field of view for in situ measurements with respect to the device cross-slot. (b) Normalized histograms showing fluorescence lifetimes from two detector channels. Fluorescence lifetimes were normalized with respect to their highest values, thereby revealing a bimodal lifetime distribution. Red represents channel 1 and green represents channel 2 (Table S1). (c) Two-dimensional spatial map of assembled oligomer fluorescence lifetimes. Color represents lifetime and is scaled the same for both (c,d). (d) Two-dimensional spatial map of unassembled oligomer fluorescence lifetimes. (e) Assembled oligomer fluorescence intensity map. Color represents intensity as the number of photon counts on the detector. (f) Unassembled oligomer fluorescence intensity map.
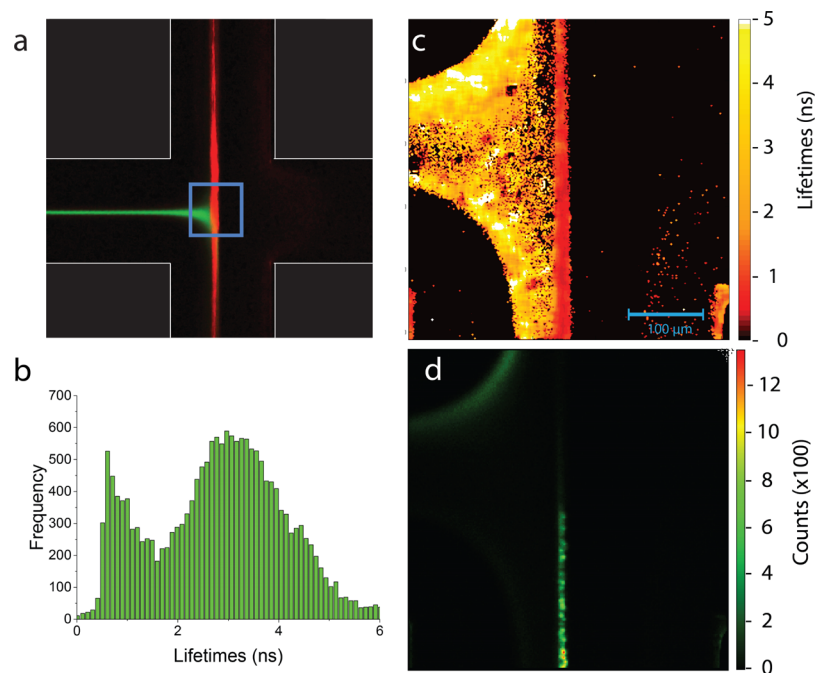

Figure 5. In situ FLIM for fluid-directed assembly of oligopeptides with PDI cores. (a) False color image of the assembly process at device cross-slot (green shows unassembled peptide and red shows assembled peptide). Blue square indicates position and field of view for in situ measurements with respect to the device cross-slot. (b) Histogram of fluorescence lifetimes shows a bimodal distribution due to unassembled and assembled oligopeptides. (c) Fluorescence lifetimes for both assembled and unassembled oligomers. (d) Fluorescence emission intensity map corresponding to the same physical region as part (c).

As in previous experiments, we inferred the generation of the aligned oligopeptide in these integrated microdevices using ex situ FLIM to analyze the assembled material collected from effluent streams. In these experiments, we studied the photophysical properties of the assembled peptide material collected in the outlet flow streams for microdevices with and without chevrons. Histograms of fluorescence lifetimes for the assembled material acquired from both simple and chevron-containing devices appear as an approximately Gaussian distribution (OPV3 peptides in Figure 6, and PDI peptides in Figure S5), indicating a highly uniformly aligned oligopeptide. Moreover, fluorescence lifetimes are observed
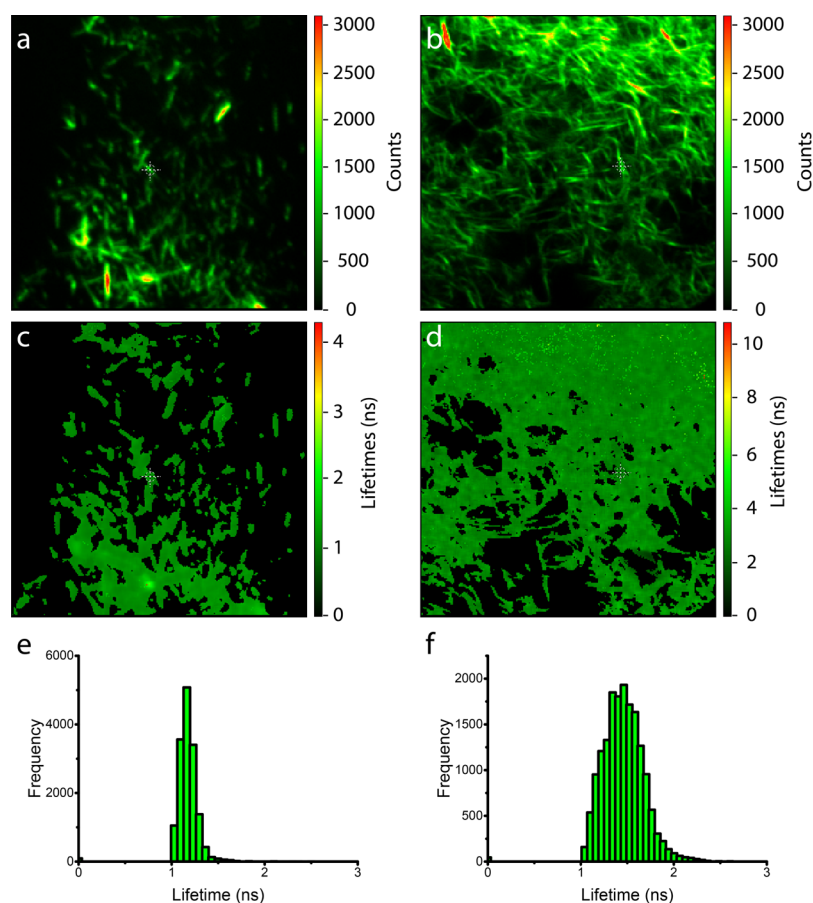
Figure 6. Fluorescence lifetimes of the assembled material collected from effluent streams in devices without and with chevrons for OPV3 synthetic peptides. (a,b) Fluorescence intensity maps of the assembled oligopeptide from a device without chevrons and a device with chevrons, respectively. (c,d) Fluorescence lifetime maps of the assembled oligopeptide from a device without chevrons and a device with chevrons, respectively. (e,f) Histograms of fluorescence lifetimes for (c,d), respectively.

to be similar for PDI materials when comparing both ex situ and, later, in situ FLIM (Figures 5 and S5). Fluorescence lifetimes of the assembled, aligned material are not observed to drastically change for materials assembled in non-chevron and chevron devices, which suggests that 3D flow focusing does not impact the integrity of the material when it is aligned. However, recent work has shown that peptide assembly can be alternatively induced through solvent evaporation and it is uncertain which mechanism underlies the assembled peptide observed ex situ on dried microscope slides.[41]

Moreover, previous work comparing unassembled to assembled materials has had to rely upon the width of the lifetime distribution as an ersatz metric to distinguish between the two.[2] These new devices with patterned channels allowed us to take advantage of the underlying physics of FLIM to quantitatively distinguish the unassembled oligomer from the aligned, assembled oligomer while the material was being assembled. FLIM probes $\pi-\pi$ stacking interactions between adjacent π-conjugated cores in order to gain insight into the supramolecular structures formed during assembly.[38] For example, the difference between pure H-stacked behavior and J-coupled behavior are not only spectrally distinct, but also exhibit different lifetime behavior. In particular, the S_0-S_1 vibration-less ground state radiative transition is symmetry-forbidden in pure H aggregates, which means that higher order transitions via phonon coupling are favored in these types of aggregates, leading to the quenched and blue-shifted

absorbance, we observe in solutions of the assembled material (Figure 1).[38,42] Furthermore, it is well established that J aggregates exhibit shorter fluorescence lifetimes compared to their unassembled monomer constituents due to a greater degree of exciton or excited state delocalization across several core species.[3,12,43,44] In this way, fluorescence lifetimes reveal additional insight into nonideal H-structures at the molecular level.

We directly probed oligopeptide assembly in continuous flow using spatially resolved in situ FLIM for both 4T- and PDI-functionalized oligopeptides (Figures 4 and 5). Figures 4a and 5a are false color images of the assembly process at the device cross-slot with a colored square indicating the position and field of view for in situ FLIM measurements. The false colors are determined by the dichroics used in each experiment as detailed in Table S1. Histograms of fluorescence lifetimes in part (b) of each figure show a clear bimodal distribution for both functional cores, with the long-time and short-time maxima distinctly corresponding to the locations of the unassembled and assembled oligopeptides, respectively. As a reference, the fluorescence lifetimes of unassembled oligopeptides with 4T and PDI cores are ~0.7 and ~3 ns, respectively. We see that all material to the left of the extensional flow axis shows the expected nanosecond scale lifetimes of the unassembled oligopeptide, and this region contains the unreacted material before it has had an opportunity to self-assemble by contacting the acid catalyst. Meanwhile, the

extensional flow axis is ablaze with sub-nanosecond lifetime fluorescence exactly where the assembly front lies. Figures 4c,d, and 5c are heat maps of the lifetimes measured for the fluorescence at each pixel. The data for Figure 4 is split across two images due to a dichroic in the microscope platform that lies in the middle of the 4T spectrum but could not be trivially removed, thus splitting the signal across two detectors. Figures 4e,f, and 5d are intensity maps showing the number of photon counts per pixel. Note that the scale for Figure 4f is an order of magnitude lower than for Figure 4e. Figure 5d clearly indicates the different spatial locations of the unassembled peptide (orange, longer lifetimes) and of the assembled peptide (red, shorter lifetimes). The marked disparity between the quality of the data in Figure 5c,d demonstrate how fluorescence lifetime information can be used to inform the assembly process despite the potentially uninformative fluorescence emission intensity data. Fluorescence lifetime shortening in the assembled structures suggests some degree of J-like aggregate behavior.[3,12,43,44] Furthermore, the number of coherently coupled molecules, known as the coherence length of an oligomer, is directly proportional to the radiative decay rate and thus inversely proportional to the fluorescence lifetime.[42,45−47] In this way, we can estimate the coherence length of the assembled fibrils to be on the order of two to five times larger than the unassembled peptide. We have thus acquired, heretofore, unobtainable evidence for the specific assembly structure based on live measurements of the material as assembly occurs.

The combination of partially H-like and J-like properties of the assembled oligopeptides raises new and interesting questions as well. This mixture of properties could arise due to tertiary or quaternary structures of joined β sheets in the assembled fibrils, as elucidated by Fitzpatrick and Debelouchina.[48] Alternatively, the assembled structure could have π-conjugated functional cores in an "offset H" type of configuration, which would lead to a slightly larger effective transition dipole and therefore a shorter lifetime compared to the unassembled peptide while retaining the H-aggregate characteristics observed in Figure 1. In order to further understand the photophysical behavior, we can consider the structure of the assembled supramolecular materials. Although the amino acid residues flanking the functional core are the primary structural determinants, β sheet formation can be altered by $\pi-\pi$ stacking interactions of the cores. The assembled supramolecular peptide structure takes the form of a twisted ribbon structure, with $\pi-\pi$ stacking interactions between adjacent π-conjugated cores and hydrogen bonding and van der Waals interactions between adjacent β sheets in the flanking peptides. Although $\pi-\pi$ stacking interactions between cores generally aid in assembly, steric interactions in amino acid side groups or core structures can influence the distance between stacked peptides. Both 4T and PDI are larger and more hydrophobic core groups compared to OPV3. From this perspective, β sheet formation for oligopeptides functionalized with larger π-conjugated cores may be hindered compared to the less bulky OPV3 core. Therefore, in some cases, these factors make it difficult to distinguish the unassembled from the assembled oligopeptides using only fluorescence emission spectra. However, we have used FLIM as an effective technique for high contrast imaging of oligopeptide assembly, regardless of fluorescence emission and absorption spectra. Notably, the fluorescence lifetime maps clearly show which regions are dominated by the presence of unassembled and assembled oligopeptide fluorescence (Figure 5), even for images in which fluorescence intensity variations make it difficult to simultaneously view under and overexposed regions.

CONCLUSIONS

In this work, we demonstrate the continuous assembly and extrusion of aligned oligopeptides using integrated microfluidics. We use finite element modeling of device geometries for flow fields and mass transport to optimize a novel microchannel device with patterned surfaces. Confocal fluorescence microscopy is used to verify that chevrons patterned into the ceilings and floors of microdevices generate a sheathed peptide monomer stream. The continuous flow facilitated by this novel design enables the collection of fluorescence emission spectra and changes in fluorescence lifetimes associated with amyloid formation. These show that oligopeptide assembly is induced in a spatially-confined 3-D reaction zone contained along the extensional flow axis of the cross-slot. Assembly occurs within a vertical distance of around 50 μm from the center-plane of the microdevice when the flow-sheathed unassembled peptide stream is directed to the interface with an opposing aqueous acid stream at a cross-slot junction. Following assembly, we further characterize the fluorescence emission properties of OPV3-, 4T-, and PDI-functionalized synthetic peptides. In this way, oligopeptides can be assembled and aligned into highly ordered structures without device clogging, thereby providing a known processing history of assembled materials collected in effluent streams. Aligned and assembled oligopeptides can be extruded in a continuous manner that is limited (in a single experiment) only by the capacity of the fluid reservoirs (in our case, glass syringes). Under proper device operation, our results suggest that there should be no limit to the number of times the external syringe pumps can be refilled in order to continue oligomer production. Using this approach, it is possible to explore the wide chemical parameter space of the peptide residue and functional core combinations in a rapid format. This microfluidic system can further be extended toward any chemical system where the designer would like to control the microscale morphology and, significantly, would like to do so in a continuous manner with high throughput deposition and patterning.

ASSOCIATED CONTENT

Ⓢ **Supporting Information**

The Supporting Information is available free of charge on the ACS Publications website at DOI: 10.1021/acs.langmuir.9b01360.

> Scanning electron microscopy images of assembled fibrils, images of continuous assembly for DFAG-4T and DFAG-PDI peptides, images demonstrating clumped peptides, transmission profile of filters and dichroic mirror for in situ FLIM system, ex situ FLIM data for peptides containing PDI cores, and observation of assembled, intact peptide materials suspended in flow (PDF)

AUTHOR INFORMATION

Corresponding Author

*E-mail: wwilson@cns.fas.harvard.edu.

ORCID Ⓞ

Charles M. Schroeder: 0000-0001-6023-2274
William L. Wilson: 0000-0003-2755-7610

■ REFERENCES

(1) Diegelmann, S. R.; Gorham, J. M.; Tovar, J. D. One-Dimensional Optoelectronic Nanostructures Derived from the Aqueous Self-Assembly of π-Conjugated Oligopeptides. *J. Am. Chem. Soc.* **2008**, *130*, 13840−13841.

(2) Marciel, A. B.; Tanyeri, M.; Wall, B. D.; Tovar, J. D.; Schroeder, C. M.; Wilson, W. L. Fluidic-Directed Assembly of Aligned Oligopeptides with π-Conjugated Cores. *Adv. Mater.* **2013**, *25*, 6398−6404.

(3) Sun, Y.; Jiang, L.; Schuermann, K. C.; Adriaens, W.; Zhang, L.; Boey, F. Y. C.; De Cola, L.; Brunsveld, L.; Chen, X. Semiconductive, One-Dimensional, Self-Assembled Nanostructures Based on Oligo-peptides with π-Conjugated Segments. *Chem.—Eur. J.* **2011**, *17*, 4746−4749.

(4) Wang, J.; Yuan, C.; Han, Y.; Wang, Y.; Liu, X.; Zhang, S.; Yan, X. Trace Water as Prominent Factor to Induce Peptide Self-Assembly: Dynamic Evolution and Governing Interactions in Ionic Liquids. *Small* **2017**, *13*, 1702175.

(5) Tovar, J. D. Supramolecular Construction of Optoelectronic Biomaterials. *Acc. Chem. Res.* **2013**, *46*, 1527−1537.

(6) Ardoña, H. A. M.; Besar, K.; Togninalli, M.; Katz, H. E. Sequence-Dependent Mechanical, Photophysical and Electrical Properties of Pi-Conjugated Peptide Hydrogelators. *J. Mater. Chem. C* **2015**, *3*, 6505.

(7) Wall, B. D.; Zacca, A. E.; Sanders, A. M.; Wilson, W. L.; Ferguson, A. L.; Tovar, J. D. Supramolecular Polymorphism: Tunable Electronic Interactions within π-Conjugated Peptide Nanostructures Dictated by Primary Amino Acid Sequence. *Langmuir* **2014**, *30*, 5946−5956.

(8) Wall, B. D.; Diegelmann, S. R.; Zhang, S.; Dawidczyk, T. J.; Wilson, W. L.; Katz, H. E.; Mao, H.-Q.; Tovar, J. D. Aligned Macroscopic Domains of Optoelectronic Nanostructures Prepared via Shear-Flow Assembly of Peptide Hydrogels. *Adv. Mater.* **2011**, *23*, 5009−5014.

(9) Wall, B. D.; Tovar, J. D. Synthesis and characterization of π-conjugated peptide-based supramolecular materials. *Pure Appl. Chem.* **2012**, *84*, 1039−1045.

(10) Liu, K.; Xing, R.; Chen, C.; Shen, G.; Yan, L.; Zou, Q.; Ma, G.; Möhwald, H.; Yan, X. Peptide-Induced Hierarchical Long-Range Order and Photocatalytic Activity of Porphyrin Assemblies. *Angew. Chem., Int. Ed.* **2015**, *54*, 500.

(11) Wang, J.; Liu, K.; Xing, R.; Yan, X. Peptide Self-Assembly: Thermodynamics and Kinetics. *Chem. Soc. Rev.* **2016**, *45*, 5589−5604.

(12) Chan, J. M. W.; Tischler, J. R.; Kooi, S. E.; Bulović, V.; Swager, T. M. Synthesis of J-Aggregating Dibenz[a,j]Anthracene-Based Macrocycles. *J. Am. Chem. Soc.* **2009**, *131*, 5659−5666.

(13) Horowitz, G. Organic Field-Effect Transistors. *Adv. Mater.* **1998**, *10*, 365.

(14) Thangawng, A. L.; Howell, P. B., Jr.; Richards, J. J.; Erickson, J. S.; Ligler, F. S. A Simple Sheath-Flow Microfluidic Device for Micro/Nanomanufacturing: Fabrication of Hydrodynamically Shaped Polymer Fibers. *Lab Chip* **2009**, *9*, 3126−3130.

(15) Zhang, S.; Greenfield, M. A.; Mata, A.; Palmer, L. C.; Bitton, R.; Mantei, J. R.; Aparicio, C.; de la Cruz, M. O.; Stupp, S. I. A Self-Assembly Pathway to Aligned Monodomain Gels. *Nat. Mater.* **2010**, *9*, 594−601.

(16) Boyd, D. A.; Shields, A. R.; Howell, P. B.; Ligler, F. S. Design and fabrication of uniquely shaped thiol-ene microfibers using a two-stage hydrodynamic focusing design. *Lab Chip* **2013**, *13*, 3105−3110.

(17) Min, S.-Y.; Kim, T.-S.; Kim, B.; Cho, H.; Noh, Y.-Y.; Yang, H.; Cho, J.; Lee, T.-W. Large-Scale Organic Nanowire Lithography and Electronics. *Nat. Commun.* **2013**, *4*, 1773.

(18) Cheng, Y.; Zheng, F.; Lu, J.; Shang, L.; Zhao, Y.; Chen, Y.; Gu, Z. Bioinspired Multicompartmental Microfibers from Microfluidics. *Adv. Mater.* **2014**, *26*, 5184.

(19) Whitesides, G. M. The Origins and the Future of Microfluidics. *Nature* **2006**, *442*, 368−373.

(20) Stroock, A. D.; Dertinger, S. K. W.; Ajdari, A.; Mezić, I.; Stone, H. A.; Whitesides, G. M. Chaotic Mixer for Microchannels. *Science* **2002**, *295*, 647.

(21) Jahn, A.; Vreeland, W. N.; Gaitan, M.; Locascio, L. E. Controlled Vesicle Self-Assembly in Microfluidic Channels with Hydrodynamic Focusing. *J. Am. Chem. Soc.* **2004**, *126*, 2674−2675.

(22) Numata, M.; Takigami, Y.; Takayama, M.; Kozawa, T.; Hirose, N. Hierarchical Supramolecular Spinning of Nanofibers in a Microfluidic Channel: Tuning Nanostructures at a Dynamic Interface. *Chem.—Eur. J.* **2012**, *18*, 13008.

(23) Elvira, K. S.; I Solvas, X. C.; Wootton, R. C. R.; Demello, A. J. The Past, Present and Potential for Microfluidic Reactor Technology in Chemical Synthesis. *Nat. Chem.* **2013**, *5*, 905.

(24) Sevim, S.; Sorrenti, A.; Franco, C.; Furukawa, S.; Pané, S.; Demello, A. J.; Puigmartí-Luis, J. Self-Assembled Materials and Supramolecular Chemistry within Microfluidic Environments: From Common Thermodynamic States to Non-Equilibrium Structures. *Chem. Soc. Rev.* **2018**, *47*, 3788.

(25) Sorrenti, A.; Rodriguez-Trujillo, R.; Amabilino, D. B.; Puigmartí-Luis, J. Milliseconds Make the Difference in the Far-from-Equilibrium Self-Assembly of Supramolecular Chiral Nanostructures. *J. Am. Chem. Soc.* **2016**, *138*, 6920−6923.

(26) Numata, M.; Sakai, R.-I. Kinetically Controllable Supra-molecular Polymerization through Synchronized Activation of Monomers. *Bull. Chem. Soc. Jpn.* **2014**, *87*, 858.

(27) Numata, M. Supramolecular Chemistry in Microflow Fields: Toward a New Material World of Precise Kinetic Control. *Chem.—Asian J.* **2015**, *10*, 2574.

(28) Howell, P. B.; Mott, D. R.; Fertig, S.; Kaplan, C. R.; Golden, J. P.; Oran, E. S.; Ligler, F. S. A microfluidic mixer with grooves placed on the top and bottom of the channel. *Lab Chip* **2005**, *5*, 524−530.

(29) Paiè, P.; Bragheri, F.; Vazquez, R. M.; Osellame, R. Straightforward 3D Hydrodynamic Focusing in Femtosecond Laser Fabricated Microfluidic Channels. *Lab Chip* **2014**, *14*, 1826−1833.

(30) Hashemi, N.; Howell, P. B., Jr.; Erickson, J. S.; Golden, J. P.; Ligler, F. S. Dynamic Reversibility of Hydrodynamic Focusing for Recycling Sheath Fluid. *Lab Chip* **2010**, *10*, 1952−1959.

(31) Lin, S.-C.; Yen, P.-W.; Peng, C.-C.; Tung, Y.-C. Single Channel Layer, Single Sheath-Flow Inlet Microfluidic Flow Cytometer with Three-Dimensional Hydrodynamic Focusing. *Lab Chip* **2012**, *12*, 3135−3141.

(32) Howell, P. B. H., Jr.; Golden, J. P.; Hilliard, L. R.; Erickson, J. S.; Mott, R.; Ligler, F. S. Two Simple and Rugged Designs for Creating Microfluidic Sheath Flow. *Lab Chip* **2008**, *8*, 1097−1103.

(33) Golden, J. P.; Justin, G. A.; Nasir, M.; Ligler, F. S. Hydrodynamic focusing-a versatile tool. *Anal Bioanal Chem* **2012**, *402*, 325−335.

(34) Nasir, M.; Ateya, D. A.; Burk, D.; Golden, J. P.; Ligler, F. S. Hydrodynamic Focusing of Conducting Fluids for Conductivity-Based Biosensors. *Biosens. Bioelectron.* **2010**, *25*, 1363−1369.

(35) Justin, G. A.; Denisin, A. K.; Nasir, M.; Shriver-lake, L. C.; Golden, J. P.; Ligler, F. S. Hydrodynamic Focusing for Impedance-Based Detection of Specifically Bound Microparticles and Cells : Implications of Fluid Dynamics on Tunable Sensitivity. *Sens. Actuators, B* **2012**, *166*, 386.

(36) Unger, M. A.; Unger, M. A.; Chou, H.; Thorsen, T.; Scherer, A.; Quake, S. R. Monolithic Microfabricated Valves and Pumps by Multilayer Soft Lithography. *Science* **2000**, *288*, 113.

(37) Duffy, D. C.; McDonald, C. J.; Schueller, O. J. A.; Whitesides, G. M. Rapid Prototyping of Microfluidic Systems in Poly-(Dimethylsiloxane). *Anal. Chem.* **1998**, *70*, 4974.

(38) Spano, F. C.; Silva, C. H- and J-Aggregate Behavior in Polymeric Semiconductors. *Annu. Rev. Phys. Chem.* **2014**, *65*, 477−500.

(39) Schroeder, C. M.; Babcock, H. P.; Shaqfeh, E. S. G.; Chu, S. Observation of Polymer Conformation Hysteresis in Extensional Flow. *Science* **2003**, *301*, 1515−1519.

(40) Mansur, E. A.; Mingxing, Y. E.; Yundong, W. A State-of-the-Art Review of Mixing in Microfluidic Mixers. *Chin. J. Chem. Eng.* **2008**, *16*, 503.

(41) Li, B.; Li, S.; Zhou, Y.; Ardoña, H. A. M.; Valverde, L. R.; Wilson, W. L.; Tovar, J. D.; Schroeder, C. M. Nonequilibrium Self-Assembly of π-Conjugated Oligopeptides in Solution. *ACS Appl. Mater. Interfaces* **2017**, *9*, 3977−3984.

(42) Spano, F. C.; Yamagata, H. Vibronic Coupling in J-Aggregates and beyond: A Direct Means of Determining the Exciton Coherence Length from the Photoluminescence Spectrum. *J. Phys. Chem. B* **2011**, *115*, 5133.

(43) Lakowicz, J. R.; Szmacinski, H.; Nowaczyk, K. Fluorescence Lifetime Imaging. *Anal. Biochem.* **1992**, *13*, 131.

(44) Suhlinga, K.; Hirvonena, L. M.; Levitta, J. A.; Chung, P. H. Fluorescence Lifetime Imaging. *Handbook of Photonics for Biomedical Engineering*; Springer, 2015.

(45) Fidder, H.; Knoester, J.; Wiersma, D. A. Superradiant Emission and Optical Dephasing in J-Aggregates. *Chem. Phys. Lett.* **1990**, *171*, 529−536.

(46) Möbius, D.; Kuhn, H. Monolayer Assemblies of Dyes to Study the Role of Thermal Collisions in Energy Transfer. *Isr. J. Chem.* **1979**, *18*, 375.

(47) Boer, S.; Wiersma, D. A. Dephasing-Induced Damping of Superradiant Emission in J-Aggregates. *Chem. Phys. Lett.* **1990**, *165*, 45−53.

(48) Fitzpatrick, A. W. P.; Debelouchina, G. T. Atomic Structure and Hierarchical Assembly of a Cross-β Amyloid Fibril. *Proc. Natl. Acad. Sci. U.S.A.* **2013**, *110*, 5468.